Inorganic Chemistry

pubs.acs.org/IC

Article

Heteroleptic Rare-Earth Tris(metallocenes) Containing a Dibenzocyclooctatetraene Dianion

Elizabeth R. Pugliese, Florian Benner, Ernesto Castellanos, Francis Delano, IV, and Selvan Demir*

Cite This: *Inorg. Chem.* 2022, 61, 2444−2454

Read Online

ACCESS | Metrics & More | Article Recommendations | Supporting Information

ABSTRACT: Isolable heteroleptic tris(metallocenes) containing five-membered and larger rings remain extremely scarce. The utilization of tripositive rare-earth-metal ions with ionic radii >1 Å allowed access to unprecedented and sterically congested dibenzocyclooctatetraenyl (dbCOT) metallocenes, [K(crypt-222)][Cp^{tet}_2RE(η^2-dbCOT)] (RE = Y (**1**), Dy (**2**); Cp^{tet} = tetramethylcyclopentadienyl), through a salt metathesis reaction involving Cp^{tet}_2RE(BPh_4) and the potassium salt of the dbCOT dianion. The solid-state structures were investigated by single-crystal X-ray diffraction, magnetometry, and IR spectroscopy and provided evidence for the first crystallographically characterized $(dbCOT)^{2-}$ anion in a complex containing d- or f-block metals. Remarkably, the $(Cp^{tet})^-$ ligands force a distortion from planarity within the $(dbCOT)^{2-}$ moiety, engendering a rare η^2-bonding motif, as opposed to the classical η^8 conformation observed in complexes bearing a $(COT)^{2-}$ ion. The η^2 coordination mode was proven crystallographically between 100 and 298 K and computationally (DFT and NBO). Furthermore, nucleus independent chemical shift (NICS) calculations uncovered significant ring current within the dbCOT ligand. The solution-state properties of **1** and **2** were analyzed via cyclic voltammetry, NMR, and UV−vis spectroscopy. Cyclic voltammograms of **1** and **2** exhibit a quasi-reversible feature indicating the accessibility of complexes with dbCOT in two oxidation states ($dbCOT^{2-/3-\bullet}$). Importantly, the dysprosium congener, **2**, is a zero-field single-molecule magnet (SMM).

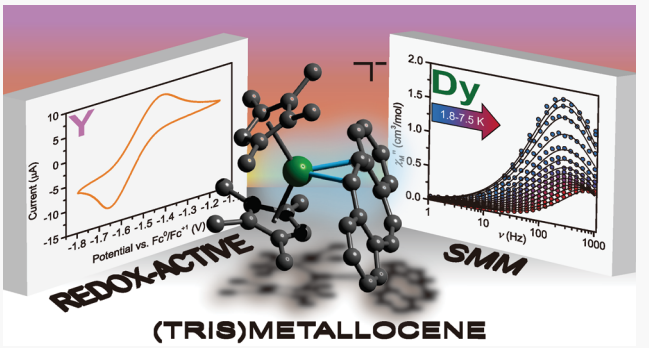

INTRODUCTION

The [8]annulene 1,3,5,7-cyclooctatetraene (COT), having alternating C−C single and double bonds, bears eight π-electrons, affording a nonplanar tub conformation in its neutral state. The addition of two electrons generates a remarkably planar and aromatic ligand, $(COT)^{2-}$, in which its large size, dianionic nature, and ability to occupy several metal coordination sites have resulted in widespread use for the organometallic synthesis of both d- and f-block compounds.[1−3] The arguably most famous organoactinide complex is uranocene, $U(COT)_2$, albeit lanthanide variants comprising the bare or functionalized COT ligand have more recently garnered vast attention for their bonding situation and physical properties.[4,5] The added stability engendered by the large number of coordination sites blocked by the $(COT)^{2-}$ ligand affords a synthon which has been used to access complexes that feature heteroleptic ligand scaffolds.[6,7] The utility of the $(COT)^{2-}$ ligand surpasses that of organometallic chemistry; in fact, the implementation of prolate Er^{III} ions gave rise to the highest blocking erbium-based single-molecule magnets (SMMs), due to the equatorial ligand field imposed by the COT-based ligands.[8−10] The modular COT scaffold allows for substitution to alter the steric bulk and solubility of the ligand. Thus, numerous derivatives with substituents varying from trimethylsilyl to cycloalkyl have been devised and employed in organometallic synthesis.[11−19] Various functionalized COT ligands (Figure 1) have been shown to be instrumental in attaining unique geometries such as double-,[20,21] triple-,[14,22] and quadruple-decker complexes.[19]

Relative to the outlined COT variants, larger arene-containing COT ligands have been underexplored.[23] A remarkable arene-functionalized COT derivative, dibenzocyclooctatetraene (dbCOT),[24,25] features two fused benzo moieties on a central COT ring. The presence of fused aromatic substituents on the COT ring increases the π surface of the molecule, which leads to enhanced π character in transition-metal (TM) catalysis.[26] The benzene rings attached to the central COT also provide additional binding sites for metals, as evidenced by the first TM-dbCOT complex, $(Cr(CO)_3)_2$(dbCOT), where the coordination of the Cr^0

Received: October 18, 2021
Published: January 18, 2022

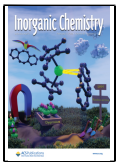

https://doi.org/10.1021/acs.inorgchem.1c03230
Inorg. Chem. 2022, 61, 2444−2454

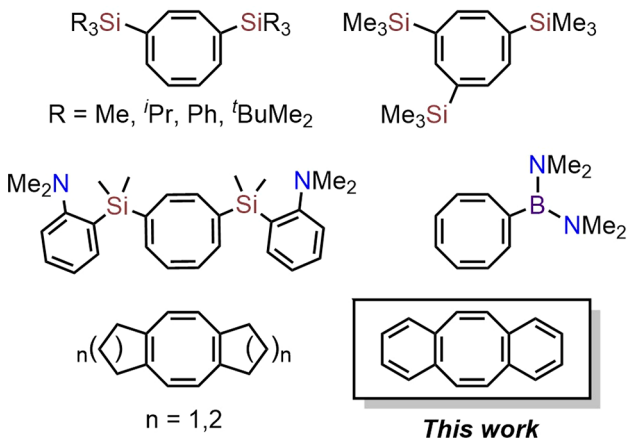

Figure 1. COT derivatives used in organometallic chemistry.

centers to the ancillary benzene rings was assigned on the basis of ^{1}H NMR spectroscopy, albeit its crystal structure remains hitherto unknown.[27]

The neutral 16-π-electron antiaromatic dbCOT ligand has been employed to synthesize complexes, mainly with precious second- and third-row d-block metals.[28] A two-electron reduction of the neutral dbCOT ligand engendered the planar dianion, $(dbCOT)^{2-}$, where its aromaticity was quantified through experimental and computational methods.[29,30] The 18-π-electron-containing $(dbCOT)^{2-}$ satisfies Huckel's rule, providing an inherent stability to the compound, similar to that of the parent $(COT)^{2-}$, and has only been crystallographically confirmed as a salt with alkali metals, such as K_2[dbCOT].[29−31] Aside from group I compounds, molecules comprising $(dbCOT)^{2-}$ dianions are unknown for the remaining elements, and the redox chemistry of dbCOT has not been exploited in coordination chemistry. With regard to the f-block metals in particular, coordination complexes with dbCOT in any oxidation state have yet to be discovered.

Herein, we describe the syntheses and structural characterization of the mononuclear yttrium and dysprosium complexes [K(crypt-222)][Cp$^{tet}_2$RE(η^2-dbCOT)], (RE = Y (**1**), Dy (**2**); crypt-222 = 2.2.2-cryptand; Cp^{tet} = tetramethylcyclopentadienyl; dbCOT = dibenzocyclooctatetraenyl). This series of compounds employing the $(dbCOT)^{2-}$ ligand is the first report on group 3 metal dbCOT complexes, as well as the first crystallographic proof of $(dbCOT)^{2-}$ coordinating to d- and f-block elements, respectively. Remarkably, these compounds represent the first set of bulky tris(metallocenes) composed of sterically demanding polyalkyl-substituted Cp rings and a large COT-based ligand. Furthermore, this work constitutes the first magnetic study of a lanthanide−dbCOT complex and the first use of the dbCOT ligand in the area of single-molecule magnetism.

EXPERIMENTAL SECTION

General Procedures. The manipulations described herein were performed under an inert nitrogen atmosphere with rigorous exclusion of air and water using Schlenk line and glovebox techniques. House nitrogen was purified through a MBraun HP-500-MO-OX gas purifier. *n*-Hexane was dried over calcium hydride. Toluene and THF were distilled over potassium. Benzophenone was used as an indicator for the dryness of THF. THF-d_8 was purchased from Sigma-Aldrich and dried over a sodium−potassium alloy. 2.2.2-Cryptand (4,7,13,16,21,24- hexaoxa-1,10-diazabicyclo[8.8.8]hexacosane) was purchased from Sigma-Aldrich and recrystallized from *n*-hexane. Potassium bis(trimethylsilylamide) (KN[Si(CH$_3$)$_3$]$_2$) was purchased from Sigma-Aldrich, dissolved in toluene, centrifuged, filtered, and recrystallized at −35 °C. Tetramethylcyclopentadiene (HCp^{tet}) was purchased from Sigma-Aldrich and dried over 4 Å sieves. Anhydrous rare-earth chlorides ($RECl_3$, RE = Dy, Y) and allylmagnesium chloride (2.0 M in THF) were purchased from Sigma-Aldrich and used as received. KCp^{tet} was synthesized by deprotonation of HCp^{tet} with K[N(SiMe$_3$)$_2$].[32] KC_8,[33] $(HNEt_3)(BPh_4)$,[34] Cp$^{tet}_2$Y(BPh$_4$),[35] and K_2dbCOT[29,30] were prepared according to literature procedures. All NMR spectra were recorded on a 500 MHz Agilent DirectDrive2 500 spectrometer at 25 °C in THF-d_8. All NMR samples were prepared under an inert atmosphere using standard NMR tubes that were sealed airtight. IR spectra were collected on solid crystalline samples with an Agilent Cary 630 FTIR spectrometer. UV−vis spectra were measured on an Agilent Cary 60 instrument, equipped with a setup consisting of fiber optics and a remote sample holder for handling in an argon-filled glovebox. A PerkinElmer 2400 Series II CHNS/O analyzer was used for CHN elemental analyses.

Synthesis of [K(crypt-222)][Cp$^{tet}_2$Y(η^2-dbCOT)] (1). *Method A (Salt Metathesis).* In a nitrogen-filled glovebox, K_2dbCOT (18.1 mg, 0.0461 mmol) was first dissolved in 2 mL of THF and then added dropwise to a stirred THF solution of Cp$^{tet}_2$Dy(BPh$_4$) (30.0 mg, 0.0461 mmol) and 2.2.2-cryptand (17.3 mg, 0.0461 mmol) to afford a dark brown solution. After 15 min of stirring, white insoluble solids, presumably $KBPh_4$, were removed via filtration. The resulting brown filtrate was evaporated to dryness under reduced pressure. Red block-shaped crystals of **1** (3.1 mg, 7% yield) suitable for X-ray analysis were grown from a concentrated THF solution at −35 °C over the course of 72 h.

Method B (Salt Metathesis Followed by Reduction). In a nitrogen-filled glovebox, K_2dbCOT (61.3 mg, 0.157 mmol) was first dissolved in 4 mL of THF and then added dropwise to a stirred THF solution of Cp$^{tet}_2$Y(BPh$_4$) (204.1 mg, 0.3135 mmol) to produce a brown solution. After 20 min, white insoluble solids, presumably $KBPh_4$, were removed by filtration. Subsequently, KC_8 (21.2 mg, 0.157 mmol) was added in the presence of 2.2.2-cryptand (59.2 mg, 0.157 mmol), giving rise to a dark red-brown solution. After 5 min of stirring, graphite was removed by filtration. The resulting brown filtrate was evaporated to dryness under reduced pressure and washed with hexane to yield a brown solid. Red block-shaped crystals of **1** (56.1 mg, 38% yield) suitable for X-ray analysis were grown from a concentrated THF solution at −35 °C over the course of 72 h. IR: 3024 w, 2957 m, 2879 s, 2812 s, 2724 m, 1582 w, 1515 m, 1503 m, 1474 m, 1438 s, 1353 vs, 1295 s, 1256 s, 1234 m, 1167 w, 1131 s, 1100 vs, 1079 vs, 1027 s, 1006 s, 949 vs, 932 vs, 826 s, 773 vs, 753 s, 729 vs, 691 s cm^{-1}. Anal. Calcd. for $C_{52}H_{74}YKN_2O_6$: C, 65.66; H, 7.84; N, 2.95. Found: C, 65.47; H, 7.82; N, 2.29.

Synthesis of [K(crypt-222)][Cp$^{tet}_2$Dy(η^2-dbCOT)] (2). *Method A (Salt Metathesis).* Complex **2** was synthesized by following the same procedure (Method A) as described for **1**, using 1 equiv each of K_2dbCOT (17.8 mg, 0.0385 mmol), Cp$^{tet}_2$Dy(BPh$_4$) (27.9 mg, 0.0385 mmol), and 2.2.2-cryptand (14.4 mg, 0.0385 mmol). **2** was isolated as brown block-shaped crystals (3.6 mg, 9% yield) from a concentrated THF solution at −35 °C over the course of 72 h.

Method B (Salt Metathesis Followed by Reduction). Complex **2** was prepared by following the same procedure (Method B) described for **1**, using 2 equiv of Cp$^{tet}_2$DyBPh$_4$ (115.1 mg, 0.1589 mmol) and 1 equiv of K_2dbCOT (31.2 mg, 0.0794 mmol) in THF. Subsequently, 1 equiv of 2.2.2-cryptand (28.6 mg, 0.0794 mmol) and 1 equiv of KC_8 (10.8 mg, 0.0794 mmol) were added. **2** was isolated as brown block-shaped crystals (21.8 mg, 27% yield) from a concentrated THF solution at −35 °C over the course of 72 h. IR: 3029 w, 2960 w, 2882 br, 2815 w, 2725 w, 1579 w, 1506 s, 1475 s, 1440 br, 1355 s, 1294 s, 1258 s, 1234 w, 1166 w, 1132 s, 1102 s, 1080 s, 1029 w, 1008 w, 949 s, 821 s, 773 s, 728 s, 692 w cm^{-1}. Anal. Calcd. for $C_{52}H_{74}DyKN_2O_6$: C, 60.95; H, 7.28; N, 2.73. Found: C, 60.97; H, 7.67; N, 2.78.

X-ray Crystallography. A red block-shaped crystal and a brown block-shaped crystal with dimensions 0.132 × 0.094 × 0.087 mm^3 and 0.458 × 0.203 × 0.171 mm^3 for **1** and **2**, respectively, were mounted on a nylon loop with Paratone oil. Data were collected using a

https://doi.org/10.1021/acs.inorgchem.1c03230
Inorg. Chem. 2022, 61, 2444−2454

XtaLAB Synergy, Dualflex, HyPix diffractometer equipped with an Oxford Cryosystems low-temperature device, operating at T = 100.0(1) and 100.1(1) K, respectively.

Data were measured using ω scans using Mo Kα radiation (microfocus sealed X-ray tube, 50 kV, 1 mA). The total number of runs and images was based on the strategy calculation from the program CrysAlisPro (Rigaku, V1.171.41.90a, 2020). Cell parameters were retrieved using CrysAlisPro (Rigaku, V1.171.41.90a, 2020) software and refined using CrysAlisPro (Rigaku, V1.171.41.90a, 2020). Data reduction was performed using the CrysAlisPro (Rigaku, V1.171.41.90a, 2020) software, which corrects for Lorentz−polarization. A numerical absorption correction based on Gaussian integration over a multifaceted crystal model empirical absorption correction using spherical harmonics was implemented in the SCALE3 ABSPACK scaling algorithm.

The structures were solved in the space group $P\bar{1}$ by using dual methods with the ShelXT (Sheldrick, 2015) structure solution program.[36] The structure was refined by least squares using version 20189/2 of XL[37] incorporated in Olex2.[38] All non-hydrogen atoms were refined anisotropically. Hydrogen atom positions were calculated geometrically and refined using the riding model.

Temperature-dependent data were measured and solved analogously to the aforementioned data. The strategy for data collection was determined by the program CrysAlisPro (Rigaku, V1.171.41.90a, 2020). The Oxford Cryosystems low-temperature device allowed for data collection at T = 100.0(1), 135.1(5), 170.0(1), 205.0(1), 240.0(1), and 279.9(1) K, respectively.

Electrochemistry. Cyclic voltammetry was performed using a Metrohm Autolab PGSTAT204 potentiostat with a glassy-carbon working electrode, platinum-wire pseudoreference electrode, and platinum wire as the counter electrode. All electrochemistry experiments were conducted within the confines of an MBraun glovebox under an argon atmosphere with an atmosphere of <0.1 ppm of O_2 and H_2O. Complexes **1** and **2** (3 mM) were dissolved in 1 mL of a 250 mM solution of [^{n}Bu$_4$N][PF$_6$] in THF. The voltammograms were referenced externally to a 3 mM solution of ferrocene. Cyclic voltammetry of the ferrocene reference solution was performed, and the Fc/Fc$^+$ redox couple was found to be 1.56 V for **1** and 1.12 V for **2**. Subsequent experiments were referenced to this value.

Magnetic Measurements. Magnetic susceptibility data were obtained on a Quantum Design MPMS3 SQUID magnetometer. A magnetic sample of [K(crypt-222)][Cp$^{tet}_2$Dy(η^2-dbCOT)] (**2**) was prepared by first drying the polycrystalline material under high vacuum and second covering the sample (9.1 mg, 8.9 × 10^{-6} mol) with molten eicosane to immobilize the crystallites prior to measurement. The sample was sealed airtight and transferred to the magnetometer.

Computational Data. All DFT calculations of **1** were performed using the Gaussian 16 program suite[39] and considered only the organometallic rare-earth complex [Cp$^{tet}_2$Y(η^2-dbCOT)]$^-$, which was calculated as an anionic singlet with a 28 in-core electron pseudopotential (ECP28MDF[40]). To determine a suitable method for the characterization of [Cp$^{tet}_2$Y(η^2-dbCOT)]$^-$, five functionals and three basis set combinations were tested. The B3LYP[41] and PBE[42] functionals were considered due to their previous implementation in characterizing the dianionic (dbCOT)$^{2-}$ ligand.[29,30] As a result, the hybrid PBE0[43] functional was assessed. The TPSS[44] and TPSSh[45] functionals were also evaluated due to their performance with transition-metal complexes.[16,17] The three basis set combinations included (a) a polarized split valence basis set (def2-SV(P))[46,47] description for all atoms, (b) the def2-SV(P)[46,47] basis set for Y and the 6-31G(d,p)[48−50] basis set for all C and H atoms, and (c) the def2-SV(P)[46,47] basis set for Y and the 6-31+G(d,p)[48−51] basis set for C and H atoms. Grimme's D3 correction was implemented in all DFT calculations to account for dispersion effects.[52]

Geometry optimizations of the anionic complex [Cp$^{tet}_2$Y(η^2-dbCOT)]$^-$ began from the crystallographic coordinates, and the structures were optimized with each of the five functionals, using the split valence 3-21G[53,54] basis set. The optimized structures were subsequently reoptimized with the following basis sets for each of the five functionals: def2-SV(P), def2-SV(P)&6-31G(d,p), and def2-SV(P)&6-31G+(d,p). Here, an analysis of the bond metrics between the experimental and computed distances was carried out, from which the hybrid PBE0 functional and def2-SV(P)&6-31G(d,p) method was determined to be most accurate on the basis of mean deviation (MD), mean square error (MSE), root-mean-square error (RMSE), and mean absolute percentage error (MAPE). Thus, a final geometry optimization was conducted of valence triple-ζ quality using the def2-TZVP&6-311G(d,p) basis sets and PBE0 functional, with the ECP28MDF pseudopotential for Y. The analytical frequencies were computed to confirm the minima structures. The nucleus independent chemical shift (NICS) calculations and natural bond orbital analyses were executed using the PBE0 def2-TZVP/6-311G(d,p) level of theory. All NBO calculations were performed using the NBO 6 program.[55] All magnetic shielding tensors of the (dbCOT)$^{2-}$ moiety were calculated with the gauge-inducing atomic orbitals (GIAO) method,[56] as implemented in the Gaussian 16 software package. The shielding tensors were calculated at the ring centroids as well as ±1.5 Å perpendicular to the ring plane in intervals of 0.25 Å. Time-dependent density functional theory (TD-DFT) calculations were performed under solvent considerations (SMD, THF) starting from the crystallographic coordinates of **1**. Only the transitions of the anion of **1**, [Cp$^{tet}_2$Y(η^2-dbCOT)]$^-$, were calculated, using the PBE0 def2-TZVP/6-311G(d,p) level of theory with the ECP28MDF pseudopotential for Y. The first 50 transitions were computed, and the molecular orbital pair with the greatest percent contribution was used to assign the transition. The crystallographic coordinates obtained from the temperature-dependent X-ray measurements were employed for geometry optimization calculations. Each structure was optimized to the PBE0 def2-TZVP&6-311G(d,p) level of theory and included the ECP28MDF pseudopotential for Y, as well as Grimme's D3 correction. The analytical frequencies of all structures were also calculated.

RESULTS AND DISCUSSION

Synthesis and Structural Characterization. Our synthetic approach to the stabilization of a heteroleptic tris(metallocene) relied on organometallic rare-earth (RE) chemistry that is largely dominated by the implementation of (polyalkyl/polysilyl)cyclopentadienyl (Cp) ligands and shaped in recent years byseveral subdisciplines such as catalysis[57] and single-molecule magnetism.[58,59] Here, the Cp ligands occupy several metal coordination sites and the substituents allow for sufficient steric bulk and increased solubility in arene solvents, benefiting the aforementioned applications. A clean and viable introduction of ligands into the realm of a metallocene unit has been particularly successful with rare-earth tetraphenylborate salts, Cp$^R_2$RE(BPh$_4$) (where R = Me$_5$, Me$_4$H), mainly due to the weakly coordinating (BPh$_4$)$^-$ anion that accommodates both the insertion of neutral ligands and a salt metathesis reaction with anionic ligands. Salt elimination reactions, with various N-heterocycles such as azobenzene,[60] azobis(pyridine),[61] bipyrimidine,[62,63] phenazine,[64,65] and tetrapyridylpyrazine[66] have proven to be fruitful synthetic routes to isolate both mono- and multinuclear RE organometallic complexes. Recently, Cp$^R_2$RE(BPh$_4$) complexes were also successfully used for the generation of rare lanthanide bismuth molecules.[67]

The bis(tetramethylcyclopentadienyl) rare-earth dbCOT compounds **1** and **2** were synthesized by treating Cp$^{tet}_2$RE(BPh$_4$) with K$_2$dbCOT(THF)$_{1.5}$ in the presence of 2.2.2-cryptand in THF (eq 1). Higher yields for **1** and **2** were achieved by the addition of KC$_8$, which formed a Cp$^{tet}_3$RE byproduct that was successfully removed by extraction with *n*-hexane (eq S1). Dark red and brown block-shaped crystals of **1** and **2**, suitable for single crystal X-ray diffraction, were

https://doi.org/10.1021/acs.inorgchem.1c03230
Inorg. Chem. 2022, 61, 2444−2454

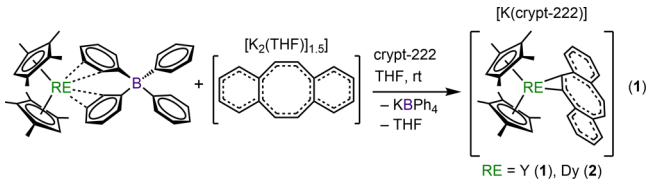

obtained from concentrated THF solutions at −35 °C over the course of 3 days in 38% and 27% yields, respectively. **1** and **2** crystallize in the $P\bar{1}$ space group and are isostructural, each exhibiting a mononuclear RE complex where the tripositive metal center is eight-coordinate with two monoanionic η^5-$(Cp^{tet})^-$ rings and is ligated by two central carbons of the dianionic η^2-$(dbCOT)^{2-}$ ligand. The potassium ion is in the outer sphere and encapsulated in the 2.2.2-cryptand. Selected interatomic distances (Å) and angles (deg) for **1** and **2** are provided in the caption for Figure 2A.

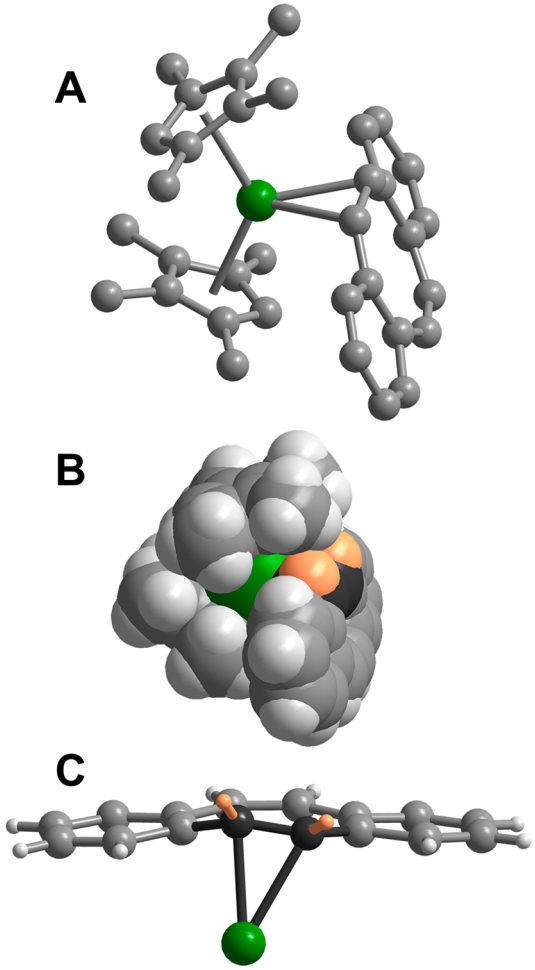

Figure 2. (A) Structure of the $[Cp^{tet}{}_2Dy(\eta^2\text{-}dbCOT)]^-$ anion in a crystal of **2**. Green and gray spheres represent Dy and C atoms, respectively. H atoms and the $[K(crypt\text{-}222)]^+$ countercation have been omitted for clarity. (B) Space-filling model of **2**. Two H and C atoms of the distorted $(dbCOT)^{2-}$ ligand, which deviate from planarity, are highlighted. (C) Distortion of $(dbCOT)^{2-}$ with H and C atoms highlighted. Complex **1** is isostructural. Selected interatomic distances (Å) and angles (deg) for **1** and **2**, respectively: $RE\text{–}Cp^{tet}{}_{cent}$ = 2.385(1), 2.396(1); $RE\text{–}C^1{}_{dbCOT}$ = 2.467(3), 2.462(3); $M\text{–}C^2{}_{dbCOT}$ = 2.566(3), 2.574(3), $Cp^{tet}{}_{cent}\text{–}RE\text{–}Cp^{tet}{}_{cent}$ = 128.7(1), 128.0(1) (where $Cp^{tet}{}_{cent}$ = Cp^{tet} ring centroid).

The X-ray diffraction data revealed the η^2 nature of the $C^1\text{–}C^8$ ring in both compounds, which was confirmed through computational methods. The two shortest $RE\text{–}C_{dbCOT}$ distances amount to 2.467(3) Å (C^1) and 2.566(3) Å (C^2) for Y and 2.462(3) Å (C^1) and 2.574(3) Å (C^2) for Dy, respectively. These are shorter than the average $RE\text{–}C_{COT}$ distances of 2.654(7) and 2.650(6) Å in $[K(18\text{-}c\text{-}6)][COT_2RE]$[9] for RE = Y and Dy, respectively, and are in good agreement with the average $Dy\text{–}C_{COT}$ distances of 2.532(8) and 2.494(33) Å in Cp*RE(COT) for Y and Dy, respectively, where Cp* = pentamethylcyclopentadienyl.[13,68] The next longest $RE\text{–}C_{dbCOT}$ distances are 2.897(3) and 2.833(4) Å for Y and Dy, respectively, which are substantially longer than those observed for RE–C interactions in allyl and aryl compounds.[62] In addition, these secondary $RE\text{–}C_{dbCOT}$ distances in **1** and **2** are also longer than the average $RE\text{–}C_{Cptet}$ distances of 2.671(2) and 2.681(3) Å, in the same molecule. The rare η^2-coordination of a COT derivative to a metal center in **1** and **2** has also been monitored in cyclooctatetraenyl-bridged porphyrinogen samarium complexes featuring bulky ancillary ligands.[69] Other than the usual η^8 mode for a COT ligand in coordination compounds, η^1, η^2, η^3, η^4, and η^6 modes have also been observed, although they are rare.[69−75]

To probe the temperature dependence of the hapticity of the $(dbCOT)^{2-}$ ligand in the solid state, a single-crystal X-ray analysis of **1** was conducted at 100, 135, 170, 205, and 298 K (Figure 3). The metrical parameters for all data are given in Table S6. Over the entire probed temperature range, the η^2 coordination mode of the $(dbCOT)^{2-}$ ligand is retained, as evidenced by the measured angles and distances. For visualization, the structures are overlaid in Figure 3G and Figure S9. Although no major differences in the hapticity of the ligand are observed, there is some variation in distance between the yttrium ion and the coordinating carbon atoms of the $(dbCOT)^{2-}$ ligand. The $Y\text{–}C_1$ and $Y\text{–}C_2$ distances are in the ranges 2.274(2)–2.570(2) and 2.470(2)–2.576(2) Å, respectively. The difference in distances is attributed to a wagging of the dbCOT ligand with rising temperatures, a consequence of the increased thermal vibrations at temperatures above 100 K. Plotting the $Y\text{–}C_1$ and $Y\text{–}C_2$ distances against temperature testifies to this structural phenomenon (Figure 3H), which is also consistent with the Y–C distances calculated from the optimized geometries at each temperature (Table S15). Notably, the distance of the Y ion to the C atom, second adjacent in range at 100 K, decreases with increasing temperatures, whereas the shortest distance of Y to the closest carbon of dbCOT remains largely unaffected over the entire probed temperature range (Figure S10). Importantly, the ligand binds in a η^2 fashion across all investigated temperatures. The next closest carbon (C16) atom of the $(dbCOT)^{2-}$ ligand to the yttrium ion is much farther away with distances of 2.890(2) and 3.321(1) Å at 100 and 298 K, respectively.

Upon complexation, the central COT ring of the $(dbCOT)^{2-}$ ligand shows a deviation from planarity in **1** and **2**, which was unexpected given the flatness of the $(dbCOT)^{2-}$ dianion in the alkali salt.[29,30] However, a remarkable ring strain is sterically imposed by the methyl groups of the cyclopentadienyl rings, as evidenced by the space-filling depiction (Figure 2B), causing the disturbance of planarity in the $(dbCOT)^{2-}$ ligand (Figure 2C). Despite the structural perturbations to the π system of the ligand, the aromatic character is retained. The $(Cp^{tet})^-$ units remain rigid, which is further attested by the $RE\text{–}Cp^{tet}{}_{cent}$ (where $Cp^{tet}{}_{cent}$ = Cp^{tet}

https://doi.org/10.1021/acs.inorgchem.1c03230
Inorg. Chem. 2022, 61, 2444−2454

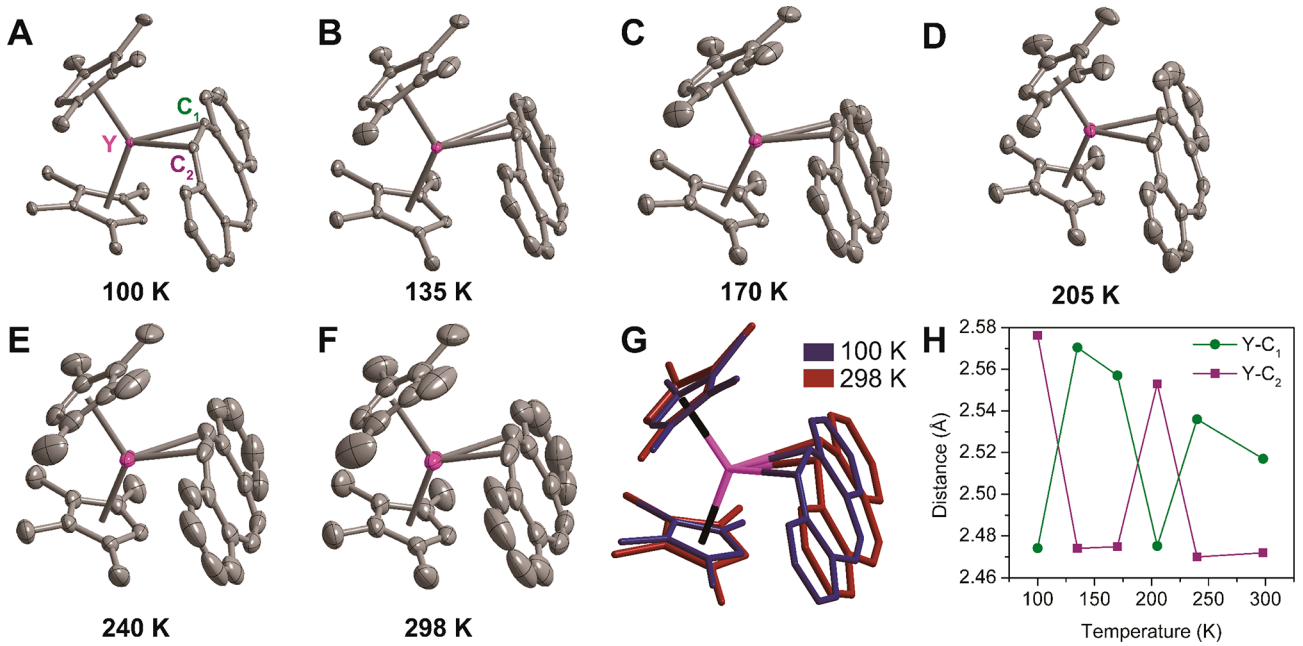

Figure 3. Structure of the $[Cp^{tet}{}_2Y(\eta^2\text{-dbCOT})]^-$ anion in a crystal of **1** at 100 K (A), 135 K (B), 170 K (C), 205 K (D), 240 K (E), and 298 K (F), respectively. (G) Overlay of the structures collected at 100 and 298 K. (H). Plots of $Y-C_1$ and $Y-C_2$ distances versus temperature.

ring centroid) distances of 2.385(1) and 2.396(1) Å in **1** and **2**, consistent with the average $RE-Cp^{tet}{}_{cent}$ distances of 2.344 and 2.365 Å detected in other rare-earth metallocenes featuring two $(\eta^5\text{-}Cp^{tet})^-$ ligands, for Y and Dy, respectively.[35,76] However, the $RE-Cp^{tet}{}_{cent}$ distances are shorter than the respective distances observed in $Cp^{tet}{}_3RE$ (2.440 Å (Y) and 2.444 Å (Dy))[35,77] and longer than the corresponding distances detected in $Cp^{tet}{}_2RE(BPh_4)$ (2.353 Å (Y) and 2.355 Å (Dy)),[35,76] likely arising from the steric bulk, which also causes the $Cp^{tet}{}_{cent}-RE-Cp^{tet}{}_{cent}$ angles to be larger (128.7° (**1**) and 128.0° (**2**) vs 120.0° (Y) and 118.0° (Dy) in $Cp^{tet}{}_3RE$).[35,77] The slight differences in all distances and angles between **1** and **2** originate from the decrease in ionic radii traversing from eight-coordinate Dy^{III} (1.027 Å) to Y^{III} (1.019 Å)[78] (Table S5).

Notably, heteroleptic tris(metallocenes) consisting of one metal center, two cyclopentadienyl derivatives, and a cyclooctatetraene ligand are extremely scarce and could only be accomplished by either implementing a large actinide ion[79] or using a substantially smaller Ln ion where the steric hindrance on the Cp ligand needed to be reduced.[80,81] In these three compounds, each metal center occupies a traditional η^5- and η^8 coordination mode as is typically observed for Cp- and COT-based ligands, respectively. To the best of our knowledge, no bulkier tris(metallocenes) have been isolated, for instance composed of alkyl-substituted Cp ligands and a larger COT ligand for any metal. The parent compounds are remarkable, as the sizes of both ligand types are significantly larger with four methyl groups on each Cp and two fused benzyl rings on the COT ligand. In addition, the employed metal center is the midsized lanthanide Dy^{III} and transition metal Y^{III}, respectively—both substantially smaller than an actinide or lanthanum ion.[78] To render coordination possible, the metal ion is forced to establish a lower coordination motif and interestingly forms this with the bulkier $(dbCOT)^{2-}$ ligand while it maintains an η^5 binding mode to the Cp rings. The driving force for the metal to a lower coordination mode to the dbCOT may be the result of the Cp ligands having been preassembled on the metal prior to reaction with K_2dbCOT. In addition, since the steric hindrance is pushed to an extreme in **1** and **2**, both are expected to function as reductants of substrates where the redox power is postulated to derive from the dbCOT ligand coordinated to the congested Dy. This hypothesis is based on the demonstrated reductive capability of U^{IV} tris(metallocenes) containing sterically more demanding alkyl substituents on Cp which cleaved chalcogenide bonds, whereas less bulky Cp rings showed no reactivity.[79]

Spectroscopic Studies. The solution behavior of **1** and **2** was probed via NMR and UV−vis spectroscopy (Figures S11, S12, S18−S20, and S23). The ^{1}H NMR spectrum of **2** features four resonances in the diamagnetic region that correlate with the $(dbCOT)^{2-}$ ligand and differ from the three resonances of the free ligand (Figures S13, S21, and S22). The additional resonance supports the η^2-coordination of the ligand. The experimental IR spectra of **1** and **2** show resonances between 1583 and 1225 cm^{-1} that coincide with the calculated and scaled DFT frequencies for **1**, which represent various symmetric and asymmetric dbCOT vibrations (Figures S14−S17). The electronic absorption spectra of **1** and **2** exhibit significant interligand $(Cp^{tet}-dbCOT)$ and intraligand (dbCOT) $\pi-\pi^*$ transitions in the UV region. Similarly, the transitions of the visible region result from LMCT transitions that were confirmed through TD-DFT calculations of **1** (Figure 4A, Figure S19, and Table S14).

Electrochemical Studies. The electrochemistry of **1** and **2** was explored via cyclic voltammetry. The cyclic voltammograms of both compounds (Figure 4B and Figures S24 and S25) indicate that mononuclear complexes with dbCOT in two oxidation states $(dbCOT^{2-/3-})$ can be obtained on the time scale of the electrochemical experiment. The individual dbCOT reduction potentials are −1.527 V (**1**) and −2.054 V (**2**) vs Fc/Fc^+ (ν = 50 mV/s), where the discrepancy may be attributed to two distinct solution-state structures possibly due to the ionic size difference of the employed metal ions.

https://doi.org/10.1021/acs.inorgchem.1c03230
Inorg. Chem. 2022, 61, 2444−2454

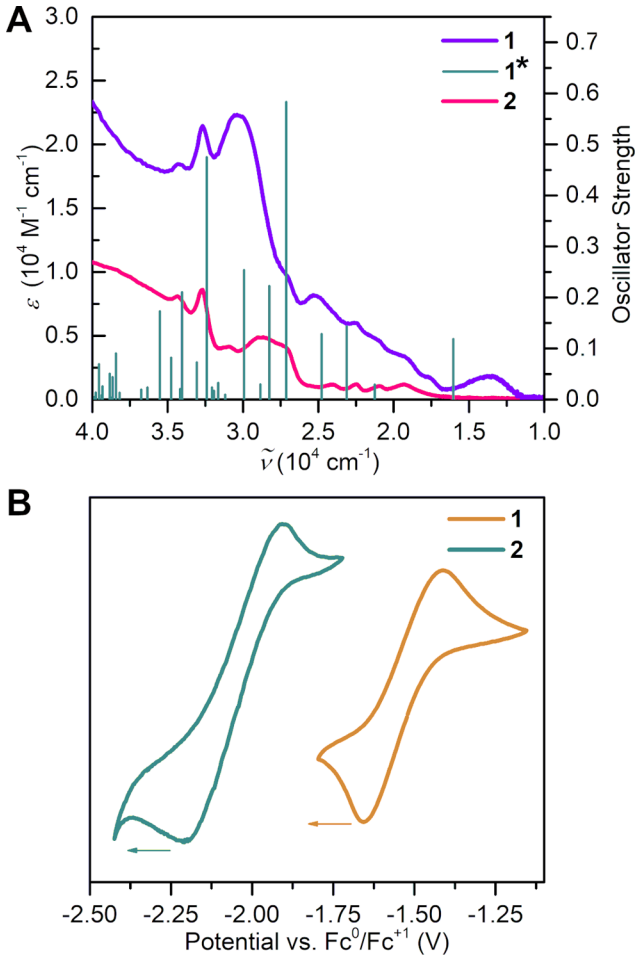

Figure 4. (A) UV−vis spectra of [K(crypt-222)][Cp^{tet}_2RE(η^2-dbCOT)] (RE = Y (**1**) (purple), Dy (**2**) (pink)) with TD-DFT computed transitions of **1** (teal, here denoted 1*), taken in THF at 3.121 × 10^{-5} and 6.105 × 10^{-5} mol/L, respectively. (B) Cyclic voltammograms of **1** (orange) and **2** (teal), measured in THF (3 mM; 250 mM [^{n}Bu$_4$N][PF$_6$]), with quasi-reversible features at −1.527 and −2.054 V, respectively.

Magnetic Studies. The magnetic properties of **2** were probed to explore its utility for SMM applications. Dc magnetic susceptibility (χ_M) data were collected for **2** from 2 to 300 K under 0.5 and 1 T dc fields. The room-temperature $\chi_M T$ value of 14.41 cm^3 K mol^{-1} at 1 T is in good agreement with the expected value for a free Dy^{III} ion (14.17 cm^3 K mol^{-1}) (Figure 5).[82] The magnetization (M) curves obtained from zero-field-cooled (zfc) and field-cooled (fc) measurements are superimposable, suggesting the absence of magnetic blocking. Field (H)-dependent magnetization data were recorded between 2 and 10 K up to 7 T (Figure S33), where even at the highest fields a saturation was not reached. The magnetization climbs with increasing magnetic field strengths to a maximum of 5.56 $N\mu_B$ (2 K). Notably, this value is slightly higher in comparison to the expected saturation magnetization for one Dy^{III} ion (5.23 $N\mu_B$), hinting at crystal/ligand field effects lifting the degeneracy of the $^6H_{15/2}$ ground state.[83] The H/T versus M curves at the respective temperatures do not overlap to a single curve. This behavior is typically attributed to significant magnetic anisotropy and/or the presence of low-lying excited states.[82] Ac magnetic susceptibility measurements revealed peaks in the

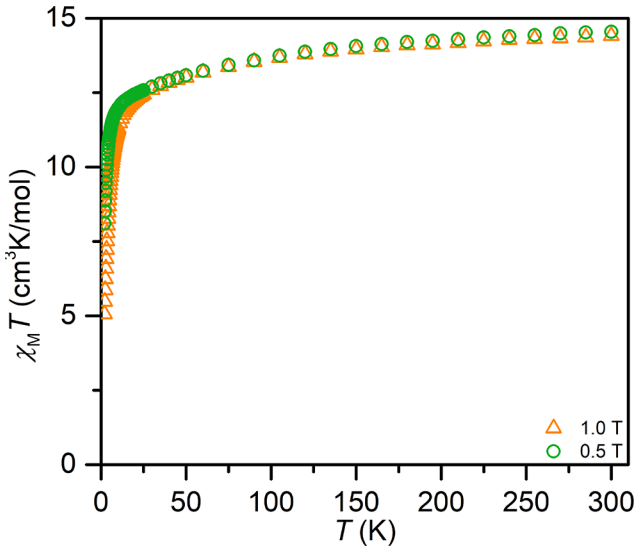

Figure 5. Variable-temperature dc magnetic susceptibility data of [K(crypt-222)][Cptet$_2$Dy(η^2-dbCOT)] (**2**), recorded under 0.5 T (green circles) and 1.0 T (orange triangles) applied dc fields.

out-of-phase component (χ_M'') between 1.8 and 7.5 K under a 0 Oe dc field (Figure 6A), indicative of slow magnetic relaxation. The data were employed to generate Cole−Cole plots at each temperature, which in the following were fit to a generalized Debye model to extract the relaxation times (τ) that ultimately provide information regarding the operative magnetic relaxation processes (Figure S31). Below 4 K, the τ values are temperature-independent, which is commonly associated with quantum tunneling of the magnetization (QTM). Hence, fitting only the temperature-dependent τ at the highest temperatures to the Arrhenius expression $\tau = \tau_0 \exp(U_{eff}/k_BT)$ describing a desirable Orbach relaxation process yielded a moderate spin-reversal barrier of U_{eff} = 20 K and τ_0 = 10^{-5} s (Figure 7). The relatively large τ_0 value suggests that relaxation is possibly occurring through a virtual excited state at these temperatures, and indeed, a satisfactory fit to all τ values was obtained by considering a QTM and a Raman relaxation process, yielding $C = 10^{-1}$ s^{-1} K^{-n} (n = 5) and τ_{QTM} = $10^{-3.3}$ s (Figure S29). The application of an optimum 1000 Oe dc field (Figure 6B,C and Figures S30 and S32) resulted in the suppression of the QTM process on the time scale of the ac measurements, where χ_M'' peak maxima are observed up to 9 K and are moving over the entire probed frequency range. Fitting the highest temperature τ values resulted in U_{eff} = 50 K and τ_0 = 10^{-6} s. An adequate fit of all τ values is attained through a single Raman process (Figure S32). The dynamic magnetic behavior may be elucidated by the orientation of the magnetic axis, which hinges on the electrostatic forces imposed by the ligand scaffold. The sandwiching of the oblate Dy^{III} ion between the negatively charged Cp ligands has been demonstrated to boost the performance of SMMs.[58,84]

The ultimate test for magnetlike behavior lies in the evaluation of variable-field magnetization measurements carried out on **2** between −4 and +4 T at 1.8 K (Figure S34). A very slight hysteresis emerges for nonzero values of H at 1.8 K, with a coercivity in the magnitude of ∼400 Oe. The loop closes at zero applied field, leaving no remanent magnetization, which is in line with our observations from the ac measurements and hints at the presence of quantum tunneling of the magnetization.

https://doi.org/10.1021/acs.inorgchem.1c03230
Inorg. Chem. 2022, 61, 2444−2454

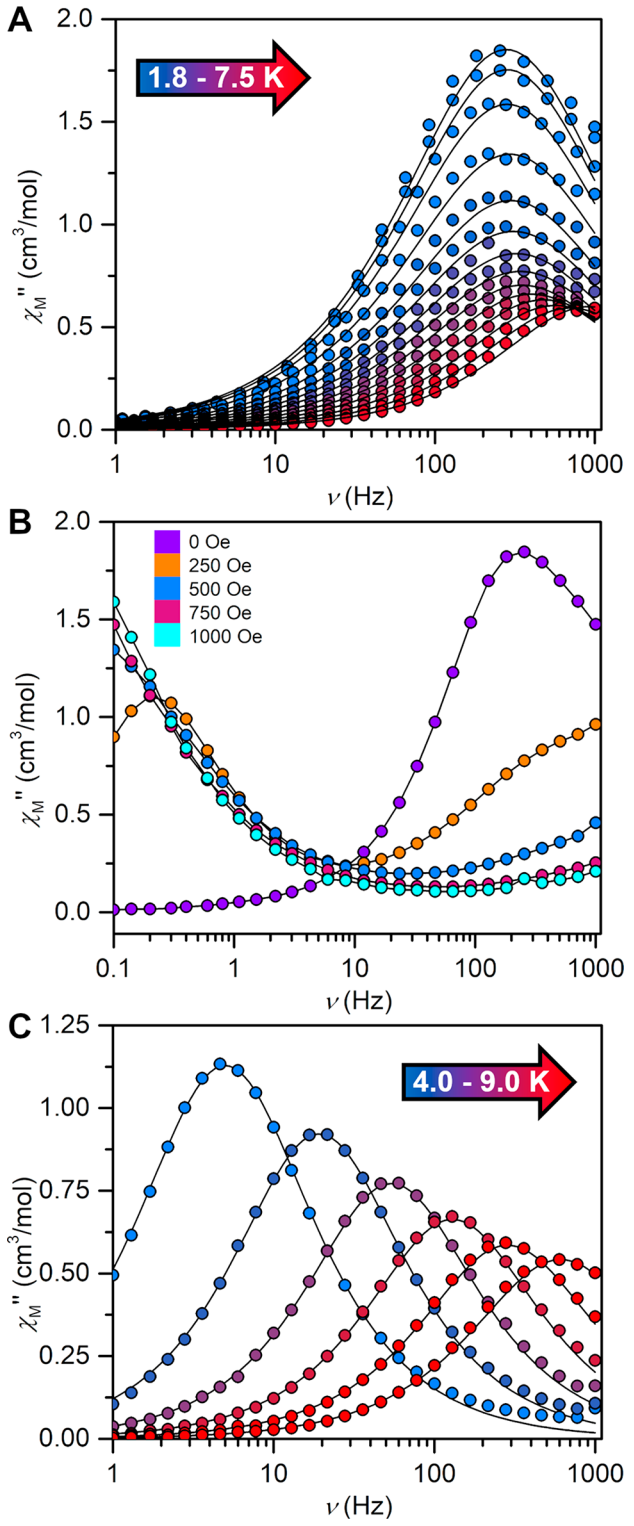

Figure 6. (A) Out-of-phase (χ_M'') components of the ac magnetic susceptibility for [K(crypt-222)][Cp^{tet}_2Dy(η^2-dbCOT)] (**2**) under zero applied dc field from 1.8 K (blue circles) to 7.5 K (red circles). Solid lines represent fits to the data, as described in the main text. (B) Out-of-phase ac magnetic susceptibility χ_M'' collected on **2** at 1.8 K under dc fields ranging from 0 to 1000 Oe, in 250 Oe increments. Solid lines are guides for the eye. (C) Out-of-phase χ_M'' components of the ac magnetic susceptibility for **2** under 1000 Oe applied dc field, from 4.0 K (blue circles) to 9.0 K (red circles). Solid lines represent fits to the data, as described in the main text.

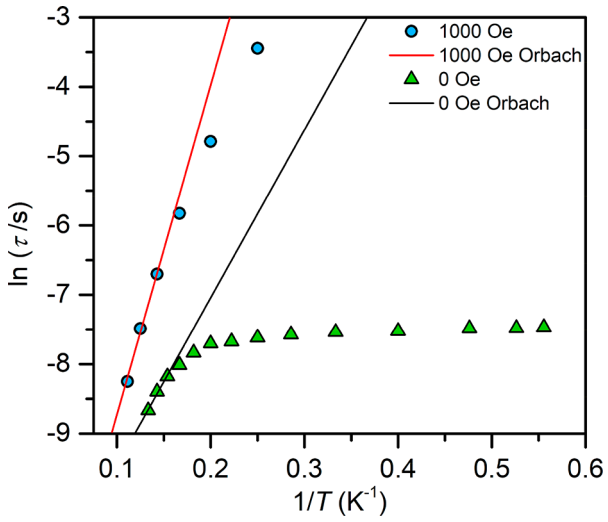

Figure 7. Arrhenius plots of relaxation time data for **2**. The black lines correspond to fits of relaxation times, τ, observed at high temperatures to the Arrhenius equation, as described in the main text.

To gain insight, the preferred orientation of the magnetic moment in **2** was calculated with the program MAGELLAN.[85] Here, we used various charge distribution schemes, as well as the Mulliken and NBO charges as obtained from the PBE0/def2-TZVP&6-311G(d,p) DFT calculations, in order to account for varying degrees of charge delocalization over the $(dbCOT)^{2-}$ ligand. If charge delocalization is considered, the $(dbCOT)^{2-}$ ligand induces only minor disruptions on the calculated magnetic axis, whereas charge localization on the COT moiety (C_8) or coordinating carbon atoms tips the axis toward the dbCOT ligand (Figure S35). The evenly distributed negative charges of the $(Cp)^-$ and $(dbCOT)^{2-}$ ligands around the Dy ion and in the equatorial plane presumably induce strong transverse anisotropy, causing mixing of m_J states that facilitates QTM. This phenomenon is known for Dy complexes containing equatorial ligands.[86−89] A localized charge distribution on the $(dbCOT)^{2-}$ ligand, however, would facilitate even stronger quantum tunneling, as the preferred orientation of the axis would destabilize the single-ion anisotropy of Dy^{III}.[90]

Computational Studies. To further investigate the electronic structure of **1**, DFT calculations were performed using the Gaussian 16 software package.[39] A suitable method for the characterization of **1** was determined by comparing the experimental and computed bond metrics of various functional and basis set combinations (Tables S8−S12). A final geometry optimization of the anionic singlet complex [Cp^{tet}_2Y(η^2-dbCOT)]$^-$ was carried out using the hybrid PBE0[43] functional and valence triple-ζ polarization basis set def2-TZVP[46] and effective core potential ECP28MDF[40] on Y. The C and H atoms were described using the valence triple-ζ basis set 6-311G(d,p) with polarization functions on all atoms.[91] The minimum structures were confirmed from the absence of imaginary frequencies, and the analytical frequencies were scaled by a factor of 0.95 to account for anharmonicity (Figures S16 and S17).

A natural bond orbital (NBO) analysis of **1** reveals an ionic bonding picture between the trivalent metal center and the coordinating $(dbCOT)^{2-}$ and $(Cp^{tet})^-$ ligands. Here, the rare η^2 coordination mode of the dbCOT ligand is supported by the presence of strongly delocalized Y−C_{dbCOT} interactions

https://doi.org/10.1021/acs.inorgchem.1c03230
Inorg. Chem. 2022, 61, 2444−2454

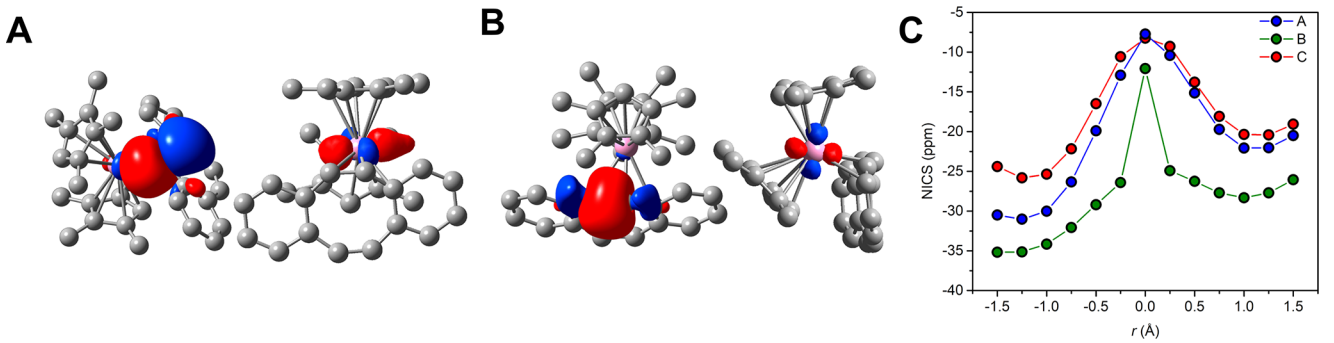

Figure 8. Depiction of select natural bond orbitals (NBOs) in $[Cp^{tet}_2Y(\eta^2\text{-dbCOT})]^-$: (A) Relevant donor and acceptor NBOs for the C^2 lone pair and Y atom, respectively; (B) relevant donor and acceptor NBOs for the C^1-C^2 bond and Y atom, respectively; (C) plot of the NICS values for $[Cp^{tet}_2Y(\eta^2\text{-dbCOT})]^-$, measured to ±1.5 Å from the centroid of the ring planes in the $(dbCOT)^{2-}$ moiety in 0.25 Å intervals. Isovalues for the carbon- and yttrium-based NBOs were set to 0.02 and 0.08, respectively.

between the π electrons of the C^1 and C^2 atoms and the vacant 5s4d hybridized and 4d orbitals of Y, respectively (Figure 8 and Figure S36). A second-order perturbation theory analysis also suggests that the significant stabilizing donations between C^1-Y and C^2-Y afford stabilization energies of 10.40 and 21.92 kcal/mol, respectively. In addition, the C^1-C^2 bond engages in a nearly equivalent stabilizing interaction with an empty 4d orbital on Y of 9.06 kcal/mol (Figure S36). This contrasts with the significantly weaker donations from the C^2-C^{16} and $C^{11}-C^{12}$ bonds with the unoccupied 4d orbitals on Y of 3.00 and 6.33 kcal/mol, respectively. Furthermore, the largest Wiberg Bond Index (WBI) values of 0.1947 and 0.0681 are ascribed to the C^1-Y and C^2-Y interactions—further supporting the $(\eta^2\text{-dbCOT})^{2-}$ assignment.

To probe the aromaticity in complex **1**, nucleus independent chemical shift (NICS)[92] calculations were performed for the six- and eight-membered rings of the $(dbCOT)^{2-}$ moiety (Figure 8 and Figure S37). The negative NICS(0) values (recorded at the centroid of each ring) of −8.2, −12.0, and −7.7 for rings A, B, and C, respectively (Figure 8), suggests that the aromatic character is retained.[92] Similarly, the average NICS(1) calculations (measured ±1 Å perpendicular to the ring planes) resulted in substantially more negative values of −26.0, −31.2, and −22.9 for rings A, B, and, C, respectively. This strong deshielding indicates the presence of significant ring currents above and below the dbCOT plane, as expected for an aromatic system. Notably, the magnitudes of the NICS(1) values were calculated to be larger below the (dbCOT) plane, possibly due to the influence of the neighboring aromatic ancillary $(Cp^{tet})^-$ ligands. However, the asymmetry of the NICS values above and below the centroids of each ring, as well as the different values between rings A and C, may be a consequence of the asymmetric coordination of the $(dbCOT)^{2-}$ ligand (Table S13). Further insight into the electronic structure of complex **1** reveals that the highest occupied molecular orbital is predominantly localized to the $(dbCOT)^{2-}$ ligand, with no contributions from the $(Cp^{tet})^-$ ligands, while the LUMO is comprised of an in-phase combination of the dianionic dbCOT π^* orbitals and the $4d_{z^2}$ orbital of Y (Figure S38).

CONCLUSION

The first series of organometallic rare-earth complexes containing the dianionic dibenzocyclooctatetraene ligand $[K(crypt\text{-}222)][Cp^{tet}_2RE(\eta^2\text{-dbCOT})]$ (RE = Y (**1**), Dy (**2**)), representing simultaneously scarce examples of a heteroleptic tris(metallocene), were synthesized and characterized. Their unique electronic structure was examined through DFT calculations, uncovering highly ionic bonding between the $(dbCOT)^{2-}$ ligand and the Y ion and confirming the unprecedented η^2 coordination mode. This unique coordination mode exists in a wide temperature range from 100 to 298 K in the solid state, as was demonstrated through the collection of six independent structures via single-crystal X-ray diffraction. These compounds constitute also the first complexation and crystallization of a dianionic dbCOT to any d- and f-block element. Furthermore, compound **2** exhibits slow magnetic relaxtion under zero dc field, yielding a moderate spin-reversal barrier. Although the Dy complex shows signatures of SMM behavior, the high anionic charge of the $(dbCOT)^{2-}$ ligand is adverse with respect to the preferred orientation of the magnetic moment, even competing with the $(Cp^{tet})^-$ framework depending on the degree of dbCOT charge delocalization. Results obtained from cyclic voltammetry and UV−vis and NMR spectroscopy imply differing solution-state dynamics for **1** and **2**, where advanced analytical methods may give insight. Notably, a reduction of **1** and **2** on the time scale of the electrochemical measurement was successful, allowing the synthetic pursuit of compounds with a dbCOT ligand in the unprecedented radical oxidation state of −3 for the dbCOT ligand. In addition, investigations toward the reductive capability of **1** and **2** derived from the sterically congested metal center and a dbCOT coordination mode of only η^2 may give rise to unusual products. In sum, future work will be directed toward the (a) synthesis and characterization of dinuclear-bridged and mononuclear $(dbCOT)^{2-}$-containing d- and f-block complexes, (b) isolation of $(dbCOT)^{3-\bullet}$ radical complexes, and (c) exploration of ligand-based redox chemistry with **1** and **2**.

ASSOCIATED CONTENT

Supporting Information

The Supporting Information is available free of charge on the ACS Publications Web site (PDF). The Supporting Information is available free of charge at https://pubs.acs.org/doi/10.1021/acs.inorgchem.1c03230.

Computational data, magnetic data, spectroscopic data, and detailed crystallographic information for **1** and **2** (PDF)

https://doi.org/10.1021/acs.inorgchem.1c03230
Inorg. Chem. 2022, 61, 2444−2454

Accession Codes

CCDC 2106661−2106662, 2129677−2129681, and 2130085 contain the supplementary crystallographic data for this paper. These data can be obtained free of charge via www.ccdc.cam.ac.uk/data_request/cif, or by emailing data_request@ccdc.cam.ac.uk, or by contacting The Cambridge Crystallographic Data Centre, 12 Union Road, Cambridge CB2 1EZ, UK; fax: +44 1223 336033.

AUTHOR INFORMATION

Corresponding Author

Selvan Demir − *Department of Chemistry, Michigan State University, East Lansing, Michigan 48823, United States;* orcid.org/0000-0001-7983-9850; Email: sdemir@chemistry.msu.edu

Authors

Elizabeth R. Pugliese − *Department of Chemistry, Michigan State University, East Lansing, Michigan 48823, United States*

Florian Benner − *Department of Chemistry, Michigan State University, East Lansing, Michigan 48823, United States*

Ernesto Castellanos − *Department of Chemistry, Michigan State University, East Lansing, Michigan 48823, United States*

Francis Delano, IV − *Department of Chemistry, Michigan State University, East Lansing, Michigan 48823, United States*

Complete contact information is available at: https://pubs.acs.org/10.1021/acs.inorgchem.1c03230

Notes

The authors declare no competing financial interest.

ACKNOWLEDGMENTS

S.D. is grateful to the Department of Chemistry at Michigan State University (MSU) for generous start-up funds. We are grateful to Dr. Richard J. Staples (MSU) for his assistance with the interpretation of the collected X-ray diffraction data. We wish to express our gratitude to Prof. Hansjörg Grützmacher (ETH) for a generous supply of chemicals. This work was supported in part through computational resources and services provided by the Institute for Cyber-Enabled Research at MSU. Funding for the single-crystal X-ray diffractometer was provided by the MRI program by the National Science Foundation under Grant No. 1919565.

REFERENCES

(1) Hodgson, K. O.; Mares, F.; Starks, D. F.; Streitwieser, A. Lanthanide(III) Complexes with Cyclooctatetraene Dianion. Synthetic Chemistry, Characterization, and Physical Properties. *J. Am. Chem. Soc.* **1973**, *95*, 8650−8658.

(2) Ishikawa, Y.; Kimura, S.; Yamamoto, K.; Murahashi, T. Bridging Coordination of Vinylarenes to Pd_3- or Pd_4 Cluster Sites. *Chem. - A Eur. J.* **2017**, *23*, 14149−14152.

(3) Evans, W. J.; Clark, R. D.; Ansari, M. A.; Ziller, J. W. Bent vs Linear Metallocenes Involving C_5Me_5 vs C_8H_8 Ligands: Synthesis, Structure, and Reactivity of the Triple-Decked $(C_5Me_5)(THF)_{(x)}$-$Sm(C_8H_8)Sm(THF)_{(x)}(C_5Me_5)$ (x = 0, 1) Complexes Including a Formal Two-Electron Oxidative Addition to a Single Lanthanide. *J. Am. Chem. Soc.* **1998**, *120*, 9555−9563.

(4) Rausch, J.; Apostolidis, C.; Walter, O.; Lorenz, V.; Hrib, C. G.; Hilfert, L.; Kühling, M.; Busse, S.; Edelmann, F. T. One Ligand Fits All: Lanthanide and Actinide Sandwich Complexes Comprising the 1,4-Bis(Trimethylsilyl)Cyclooctatetraenyl (=COT″) Ligand. *New J. Chem.* **2015**, *39*, 7656−7666.

(5) Evans, W. J.; Johnston, M. A.; Greci, M. A.; Ziller, J. W. Synthesis, Structure, and Reactivity of Unsolvated Triple-Decked Bent Metallocenes of Divalent Europium and Ytterbium. *Organometallics* **1999**, *18*, 1460−1464.

(6) Schumann, H.; Koehn, R. D.; Reier, F. W.; Dietrich, A.; Pickardt, J. Organometallic Compounds of the Lanthanides. 48. Cyclooctatetraenyl Pentamethylcyclopentadienyl Derivatives of the Rare Earths. *Organometallics* **1989**, *8*, 1388−1392.

(7) Münzfeld, L.; Schoo, C.; Bestgen, S.; Moreno-Pineda, E.; Köppe, R.; Ruben, M.; Roesky, P. W. Synthesis, Structures and Magnetic Properties of $[(C_9H_9)Ln[(C_8H_8)]$ Super Sandwich Complexes. *Nat. Commun.* **2019**, *10*, 1−7.

(8) Le Roy, J. J.; Ungur, L.; Korobkov, I.; Chibotaru, L. F.; Murugesu, M. Coupling Strategies to Enhance Single-Molecule Magnet Properties of Erbium−Cyclooctatetraenyl Complexes. *J. Am. Chem. Soc.* **2014**, *136*, 8003−8010.

(9) Meihaus, K. R.; Long, J. R. Magnetic Blocking at 10 K and a Dipolar-Mediated Avalanche in Salts of the Bis(η^8-Cyclooctatetraenide) Complex $[Er(COT)_2]^-$. *J. Am. Chem. Soc.* **2013**, *135*, 17952−17957.

(10) Hilgar, J. D.; Bernbeck, M. G.; Flores, B. S.; Rinehart, J. D. Metal-Ligand Pair Anisotropy in a Series of Mononuclear Er-COT Complexes. *Chem. Sci.* **2018**, *9*, 7204−7209.

(11) Le Roy, J. J.; Ungur, L.; Korobkov, I.; Chibotaru, L. F.; Murugesu, M. Coupling Strategies to Enhance Single-Molecule Magnet Properties of Erbium-Cyclooctatetraenyl Complexes. *J. Am. Chem. Soc.* **2014**, *136*, 8003−8010.

(12) Hiller, M.; Maier, M.; Wadepohl, H.; Enders, M. Paramagnetic NMR Analysis of Substituted Biscyclooctatetraene Lanthanide Complexes. *Organometallics* **2016**, *35*, 1916−1922.

(13) Lorenz, V.; Liebing, P.; Böhme, M.; Buchholz, A.; Plass, W.; Geue, N.; Hilfert, L.; Busse, S.; Engelhardt, F.; Hrib, C. G.; Edelmann, F. T. Lanthanide(III) Sandwich and Half-Sandwich Complexes with Bulky Cyclooctatetraenyl Ligands: Synthesis, Structures, and Magnetic Properties. Eur. *J. Inorg. Chem.* **2017**, *2017*, 4840−4849.

(14) Lorenz, V.; Blaurock, S.; Hrib, C. G.; Edelmann, F. T. The First Linear, Homoleptic Triple-Decker Sandwich Complex of an f-Element: A Molecular Model for Organolanthanide Nanowires. *Organometallics* **2010**, *29*, 4787−4789.

(15) Wetzel, T. G.; Roesky, P. W. A. Functionalized Cyclooctatetraene as Ligand in Organolanthanide Chemistry. *Organometallics* **1998**, *17*, 4009−4013.

(16) Edelmann, A.; Lorenz, V.; Hrib, C. G.; Hilfert, L.; Blaurock, S.; Edelmann, F. T. Steric Effects in Lanthanide Sandwich Complexes Containing Bulky Cyclooctatetraenyl Ligands. *Organometallics* **2013**, *32*, 1435−1444.

(17) Edelmann, A.; Hrib, C. G.; Blaurock, S.; Edelmann, F. T. New Sandwich Complexes of Di- and Trivalent Ytterbium: Reduction of Yb(3+) by a Bulky Cyclooctatetraenyl Dianion. *J. Organomet. Chem.* **2010**, *695*, 2732−2737.

(18) Braunschweig, H.; Damme, A.; Dück, K.; Krummenacher, I.; Paprocki, V.; Radacki, K.; Ramler, J.; Schiller, C.; Schneider, C. Boryl- and Silyl-Substituted Mixed Sandwich Compounds of Scandium. *Chem. Eur. J.* **2018**, *24*, 2403−2409.

(19) Münzfeld, L.; Hauser, A.; Hädinger, P.; Weigend, F.; Roesky, P. W. The Archetypal Homoleptic Lanthanide Quadruple-Decker — Synthesis, Mechanistic Studies, and Quantum Chemical Investigations. *Angew. Chem. - Int. Ed.* **2021**, *60*, 24493−24499.

(20) Meihaus, K. R.; Long, J. R. Magnetic Blocking at 10 K and a Dipolar-Mediated Avalanche in Salts of the Bis(η^8-Cyclooctatetraenide) Complex $[Er(COT)_2]^-$. *J. Am. Chem. Soc.* **2013**, *135*, 17952−17957.

(21) Rausch, J.; Apostolidis, C.; Walter, O.; Lorenz, V.; Hrib, C. G.; Hilfert, L.; Kühling, M.; Busse, S.; Edelmann, F. T. One Ligand Fits All: Lanthanide and Actinide Sandwich Complexes Comprising the 1,4-Bis(Trimethylsilyl)Cyclooctatetraenyl (=COT″) Ligand. *New J. Chem.* **2015**, *39*, 7656−7666.

(22) Le Roy, J. J.; Ungur, L.; Korobkov, I.; Chibotaru, L. F.; Murugesu, M. Coupling Strategies to Enhance Single-Molecule Magnet Properties of Erbium−Cyclooctatetraenyl Complexes. *J. Am. Chem. Soc.* **2014**, *136*, 8003−8010.
(23) Streitwieser, A.; Kluttz, R. Q.; Smith, K. A.; Luke, W. D. Dibenzouranocene and Related Compounds. *Organometallics* **1983**, *2*, 1873−1877.
(24) Fieser, L. F.; Pechet, M. M. 1,2,5,6-Dibenzcycloöctatetraene. *J. Am. Chem. Soc.* **1946**, *68*, 2577−2580.
(25) Griffin, C. E.; Peters, J. A. A Convenient Synthesis of 1,2,5,6-Dibenzocyclooctatetraene. *J. Org. Chem.* **1963**, *28*, 1715−1716.
(26) Läng, F.; Breher, F.; Stein, D.; Grützmacher, H. Chiral Olefins as Steering Ligands: Syntheses of C1-Symmetric Dibenzo[a,e]-Cyclooctenes (Rdbcot). *Organometallics* **2005**, *24*, 2997−3007.
(27) Müller, J.; Göser, P.; Elian, M. Dibenzo[u,e]cyclooctene Complexes of Chromium and Molybdenum. *Angew. Chem. - Int. Ed.* **1969**, *8*, 374−375.
(28) Spiess, S.; Welter, C.; Franck, G.; Taquet, J. P.; Helmchen, G. Iridium-Catalyzed Asymmetric Allylic Substitutions-Very High Regioselectivity and Air Stability with a Catalyst Derived from Dibenzo[a,e]Cyclooctatetraene and a Phosphoramidite. *Angew. Chem. - Int. Ed.* **2008**, *47*, 7652−7655.
(29) Bloch, J.; Kradolfer, S.; L. Gianetti, T.; Ostendorf, D.; Dey, S.; Mougel, V.; Grützmacher, H. Synthesis and Characterization of Ion Pairs between Alkaline Metal Ions and Anionic Anti-Aromatic and Aromatic Hydrocarbons with π-Conjugated Central Seven- and Eight-Membered Rings. *Molecules* **2020**, *25*, 4742−4765.
(30) Zhu, Y.; Zhou, Z.; Wei, Z.; Petrukhina, M. A. Two-Fold Reduction of Dibenzo[a,e]Cyclooctatetraene with Group 1 Metals: From Lithium to Cesium. *Organometallics* **2020**, *39*, 4688−4695.
(31) Sygula, A.; Fronczek, F. R.; Rabideau, P. W. The First Example of H_8 Coordination of Lithium Cations with a Cyclooctatetraene Dianion: Crystal Structure of Li_2(Dibenzo[a,e]Cyclooctatetraene)-$(TMEDA)_2$. *J. Organomet. Chem.* **1996**, *526*, 389−391.
(32) Evans, W. J.; Lee, D. S.; Johnston, M. A.; Ziller, J. W. The Elusive $(C_5Me_5)_3Lu$: Its Synthesis and $LnZ_3/K/N_2$ Reactivity. *Organometallics* **2005**, *24*, 6393−6397.
(33) Bergbreiter, D. E.; Killough, J. M. Reactions of Potassium-Graphite. *J. Am. Chem. Soc.* **1978**, *100*, 2126−2134.
(34) Barker, B. J.; Huffman, H. L.; Sears, P. G. Conductance Behavior of Tetraalkylammonium Salts in 3-Tert-Butyl-2-Oxazolidone at 25°. *J. Phys. Chem.* **1974**, *78*, 2689−2693.
(35) Lorenz, S. E.; Schmiege, B. M.; Lee, D. S.; Ziller, J. W.; Evans, W. J. Synthesis and Reactivity of Bis(Tetramethylcyclopentadienyl) Yttrium Metallocenes Including the Reduction of $[(Me_3Si)_2N]$ with $[(C_5Me_4H)_2Y(THF)]_2(\mu\text{-}\eta^2\text{:}\eta^2\text{-}N_2)$. *Inorg. Chem.* **2010**, *49*, 6655−6663.
(36) Sheldrick, G. M. SHELXT - Integrated Space-Group and Crystal-Structure Determination. *Acta Crystallogr., Sect. A* **2015**, *71*, 3−8.
(37) Sheldrick, G. Crystal Structure Refinement with SHELXL. *Acta Crystallogr. Sect. C* **2015**, *71*, 3−8.
(38) Dolomanov, O. V.; Bourhis, L. J.; Gildea, R. J.; Howard, J. A. K.; Puschmann, H. OLEX2: A Complete Structure Solution, Refinement and Analysis Program. *J. Appl. Crystallogr.* **2009**, *42*, 339−341.
(39) Frisch, M. J.; Trucks, G. W.; Schlegel, H. B.; Scuseria, G. E.; Robb, M. A.; Cheeseman, J. R.; Scalmani, G.; Barone, V.; Petersson, G. A.; Nakatsuji, H.; Li, X.; Caricato, M.; Marenich, A. V.; Bloino, J.; Janesko, B. G.; Gomperts, R.; Mennucci, B.; Hratchian, H. P.; Ortiz, J. V.; Izmaylov, A. F.; Sonnenberg, J. L.; Williams-Young, D.; Ding, F.; Lipparini, F.; Egidi, F.; Goings, J.; Peng, B.; Petrone, A.; Henderson, T.; Ranasinghe, D.; Zakrzewski, V. G.; Gao, J.; Rega, N.; Zheng, G.; Liang, W.; Hada, M.; Ehara, M.; Toyota, K.; Fukuda, R.; Hasegawa, J.; Ishida, M.; Nakajima, T.; Honda, Y.; Kitao, O.; Nakai, H.; Vreven, T.; Throssell, K.; Montgomery, J. A., Jr.; Peralta, J. E.; Ogliaro, F.; Bearpark, M. J.; Heyd, J. J.; Brothers, E. N.; Kudin, K. N.; Staroverov, V. N.; Keith, T. A.; Kobayashi, R.; Normand, J.; Raghavachari, K.; Rendell, A. P.; Burant, J. C.; Iyengar, S. S.; Tomasi, J.; Cossi, M.; Millam, J. M.; Klene, M.; Adamo, C.; Cammi, R.; Ochterski, J. W.; Martin, R. L.; Morokuma, K.; Farkas, O.; Foresman, J. B.; Fox, D. J. *Gaussian 16*; Gaussian Inc.: 2016.
(40) Peterson, K. A.; Figgen, D.; Dolg, M.; Stoll, H. Energy-Consistent Relativistic Pseudopotentials and Correlation Consistent Basis Sets for the 4d Elements Y-Pd. *J. Chem. Phys.* **2007**, *126*, 124101.
(41) Becke, A. D. Density-Functional Thermochemistry. III. The Role of Exact Exchange. *J. Chem. Phys.* **1993**, *98*, 5648−5652.
(42) Perdew, J. P.; Burke, K.; Ernzerhof, M. Generalized Gradient Approximation Made Simple. *Phys. Rev. Lett.* **1996**, *77*, 3865−3868.
(43) Adamo, C.; Barone, V. Toward Reliable Density Functional Methods without Adjustable Parameters: The PBE0 Model. *J. Chem. Phys.* **1999**, *110*, 6158−6170.
(44) Tao, J.; Perdew, J. P.; Staroverov, V. N.; Scuseria, G. E. Climbing the Density Functional Ladder: Nonempirical Meta−Generalized Gradient Approximation Designed for Molecules and Solids. *Phys. Rev. Lett.* **2003**, *91*, 3−6.
(45) Staroverov, V. N.; Scuseria, G. E.; Tao, J.; Perdew, J. P. Comparative Assessment of a New Nonempirical Density Functional: Molecules and Hydrogen-Bonded Complexes. *J. Chem. Phys.* **2003**, *119*, 12129−12137.
(46) Weigend, F.; Ahlrichs, R. Balanced Basis Sets of Split Valence, Triple Zeta Valence and Quadruple Zeta Valence Quality for H to Rn: Design and Assessment of Accuracy. *Phys. Chem. Chem. Phys.* **2005**, *7*, 3297−3305.
(47) Andrae, D.; Häußermann, U.; Dolg, M.; Stoll, H.; Preuß, H. Energy-Adjusted ab Initio Pseudopotentials for the Second and Third Row Transition Elements. *Theor. Chim. Acta* **1990**, *77*, 123−141.
(48) Ditchfield, R.; Hehre, W. J.; Pople, J. A. Self-Consistent Molecular-Orbital Methods. IX. An Extended Gaussian-Type Basis for Molecular-Orbital Studies of Organic Molecules. *J. Chem. Phys.* **1971**, *54*, 724−728.
(49) Hehre, W. J.; Ditchfield, K.; Pople, J. A. Self-Consistent Molecular Orbital Methods. XII. Further Extensions of Gaussian-Type Basis Sets for Use in Molecular Orbital Studies of Organic Molecules. *J. Chem. Phys.* **1972**, *56*, 2257−2261.
(50) Hariharan, P. C.; Pople, J. A. The Influence of Polarization Functions on Molecular Orbital Hydrogenation Energies. *Theor. Chim. Acta* **1973**, *28*, 213−222.
(51) Clark, T.; Chandrasekhar, J.; Spitznagel, G. W.; Schleyer, P. V. R. Efficient Diffuse Function-Augmented Basis Sets for Anion Calculations. III. The 3-21+G Basis Set for First-Row Elements, Li-F. *J. Comput. Chem.* **1983**, *4*, 294−301.
(52) Grimme, S.; Antony, J.; Ehrlich, S.; Krieg, H. A Consistent and Accurate Ab Initio Parametrization of Density Functional Dispersion Correction (DFT-D) for the 94 Elements H-Pu. *J. Chem. Phys.* **2010**, *132*, 154104.
(53) Dobbs, K. D.; Hehre, W. J. Molecular Orbital Theory of the Properties of Inorganic and Organometallic Compounds. 6. Extended Basis Sets for Second-Row Transition Metals. *J. Comput. Chem.* **1987**, *8*, 880−893.
(54) Binkley, J. S.; Pople, J. A.; Hehre, W. J. Self-Consistent Molecular Orbital Methods. 21. Small Split-Valence Basis Sets for First-Row Elements. *J. Am. Chem. Soc.* **1980**, *102*, 939−947.
(55) Glendening, E. D.; Landis, C. R.; Weinhold, F. NBO 6.0: Natural Bond Orbital Analysis Program. *J. Comput. Chem.* **2013**, *34*, 1429−1437.
(56) Wolinski, K.; Hinton, J. F.; Pulay, P. Efficient Implementation of the Gauge-Independent Atomic Orbital Method for NMR Chemical Shift Calculations. *J. Am. Chem. Soc.* **1990**, *112*, 8251−8260.
(57) Nishiura, M.; Guo, F.; Hou, Z. Half-Sandwich Rare-Earth-Catalyzed Olefin Polymerization, Carbometalation, and Hydroarylation. *Acc. Chem. Res.* **2015**, *48*, 2209−2220.
(58) Guo, F. S.; Day, B. M.; Chen, Y. C.; Tong, M. L.; Mansikkamäki, A.; Layfield, R. A. Magnetic Hysteresis up to 80 K in a Dysprosium Metallocene Single-Molecule Magnet. *Science* **2018**, *362*, 1400−1403.

https://doi.org/10.1021/acs.inorgchem.1c03230
Inorg. Chem. 2022, 61, 2444−2454

(59) Day, B. M.; Guo, F.-S.; Layfield, R. A. Cyclopentadienyl Ligands in Lanthanide Single-Molecule Magnets: One Ring To Rule Them All? *Acc. Chem. Res.* **2018**, *51*, 1880−1889.
(60) Berg, D. J.; Boncella, J. M.; Andersen, R. A. Preparation of Coordination Compounds of Cp^*_2Yb with Heterocyclic Nitrogen Bases: Examples of Antiferromagnetic Exchange Coupling across Bridging Ligands. *Organometallics* **2002**, *21*, 4622−4631.
(61) Delano, F., IV; Castellanos, E.; McCracken, J.; Demir, S. A Rare Earth Metallocene Containing a 2,2′-Azopyridyl Radical Anion. *Chem. Sci.* **2021**, *12*, 15219−15228.
(62) Demir, S.; Zadrozny, J. M.; Nippe, M.; Long, J. R. Exchange Coupling and Magnetic Blocking in Bipyrimidyl Radical-Bridged Dilanthanide Complexes. *J. Am. Chem. Soc.* **2012**, *134*, 18546−18549.
(63) Gould, C. A.; Mu, E.; Vieru, V.; Darago, L. E.; Chakarawet, K.; Gonzalez, M. I.; Demir, S.; Long, J. R. Substituent Effects on Exchange Coupling and Magnetic Relaxation in 2,2′-Bipyrimidine Radical-Bridged Dilanthanide Complexes. *J. Am. Chem. Soc.* **2020**, *142*, 21197−21209.
(64) Evans, W. J.; Walensky, J. R.; Champagne, T. M.; Ziller, J. W.; DiPasquale, A. G.; Rheingold, A. L. Displacement, Reduction, and Ligand Redistribution Reactivity of the Cationic Mono-C_5Me_5 Ln^{2+} Complexes $(C_5Me_5)Ln(BPh_4)$ (Ln = Sm, Yb). *J. Organomet. Chem.* **2009**, *694*, 1238−1243.
(65) Macdonald, M. R.; Ziller, J. W.; Evans, W. J. Coordination and Reductive Chemistry of Tetraphenylborate Complexes of Trivalent Rare Earth Metallocene Cations, $[(C_5Me_5)_2Ln][(\mu\text{-}Ph)_2BPh_2]$. *Inorg. Chem.* **2011**, *50*, 4092−4106.
(66) Demir, S.; Nippe, M.; Gonzalez, M. I.; Long, J. R. Exchange Coupling and Magnetic Blocking in Dilanthanide Complexes Bridged by the Multi-Electron Redox-Active Ligand 2,3,5,6-Tetra(2-Pyridyl)-Pyrazine. *Chem. Sci.* **2014**, *5*, 4701−4711.
(67) Zhang, P.; Benner, F.; Chilton, N. F.; Demir, S. Organometallic Lanthanide Bismuth Cluster Single-Molecule Magnets. *Chem.* **2021**, DOI: 10.1061/j.chempr.2021.11.007.
(68) Jiang, S.-D.; Liu, S.-S.; Zhou, L.-N.; Wang, B.-W.; Wang, Z.-M.; Gao, S. Series of Lanthanide Organometallic Single-Ion Magnets. *Inorg. Chem.* **2012**, *51*, 3079−3087.
(69) Frey, A. S. P.; Gardiner, M. G.; Stringer, D. N.; Yates, B. F.; George, A. V.; Jensen, P.; Turner, P. Buckling under Strain: Relief of Steric Pressure Occurs Differently for Samarium(III) Porphyrinogen Complexes of the π-Bound Auxiliary Ligands Cyclopentadienyl and Cyclooctatetraenediyl. *Organometallics* **2007**, *26*, 1299−1302.
(70) Edwin, J.; Geiger, W. E.; Rheingold, A. L. Structural Rearrangements in the Two-Electron Oxidations of Dimetal Cyclo-octatetraene Compounds. Structure of the 34-Electron Triple-Decker Dication. *J. Am. Chem. Soc.* **1984**, *106*, 3052−3053.
(71) Bieri, J. H.; Egolf, T.; Von Philipsborn, W.; Piantini, U.; Prewo, R.; Ruppli, U.; Salzer, A. The Reactivity of Complexed Carbocycles. 16.Structural and NMR Spectroscopic Studies of Cyclooctatetraene as a Bridging Ligand: Five Different Bonding Modes in Dimetallic Complexes. *Organometallics* **1986**, *5*, 2413−2425.
(72) Highcock, W. J.; Mills, R. M.; Spencer, J. L.; Woodward, P. The Relative Stability of Cyclo-Octatetraene Complexes of Zirconium(II) and Zirconium(IV); X-Ray Crystal Structure of $[Zr(\eta\text{-}C_3H_5)(\eta\text{-}C_3Me_5)\text{-}(1\text{-}4\text{-}\eta\text{-}C_8H_8)]$. *J. Chem. Soc. Chem. Commun.* **1982**, *1982*, 128−129.
(73) Hemond, R. C.; Hughes, R. P.; Rheingold, A. L. Synthesis of η^6-Octafluorocyclooctatetraene and η^6-Cyclooctatetraene Complexes of Manganese(I). Molecular Structures of $[Mn\text{-}C_5R_5\text{-}C_8X_8)]$ (R = H, Me, X = F; R = Me, X = H). *Organometallics* **1989**, *8*, 1261−1269.
(74) Evans, W. J.; Nyce, G. W.; Ziller, J. W. Formal Three-Electron Reduction by an f-Element Complex: Formation of $[\{(C_5Me_5)\text{-}U\}_2(C_8H_8)]$ from Cyclooctatetraene and $[(C_5Me_5)_3U]$. *Angew. Chem. - Int. Ed.* **2000**, *39*, 240−242.
(75) Heck, J.; Lange, G.; Malessa, M.; Boese, R.; Blaser, D. Cooperative Effects in Pi-Ligand Bridged Dinuclear Complexes, Part XXI - Synfacially Structured [(CpRuCot] - What a Difference the Coordination Side Makes! *Chem. Eur. J.* **1999**, *5*, 659−668.
(76) Demir, S.; Gonzalez, M. I.; Darago, L. E.; Evans, W. J.; Long, J. R. Giant Coercivity and High Magnetic Blocking Temperatures for − Radical-Bridged Dilanthanide Complexes upon Ligand Dissociation. *Nat. Commun.* **2017**, *8*, 2144.
(77) Jenkins, T. F.; Woen, D. H.; Mohanam, L. N.; Ziller, J. W.; Furche, F.; Evans, W. J. Tetramethylcyclopentadienyl Ligands Allow Isolation of Ln(II) Ions across the Lanthanide Series in $[K(2.2.2\text{-}Cryptand)][(C_5Me_4H)_3Ln]$ Complexes. *Organometallics* **2018**, *37*, 3863−3873.
(78) Shannon, R. D. Revised Effective Ionic Radii and Systematic Studies of Interatomic Distances in Halides and Chalcogenides. *Acta Crystallogr., Sect. A* **1976**, *32*, 751−767.
(79) Takase, M. K.; Ziller, J. W.; Evans, W. J. The Importance of a Single Methyl Group in Determining the Reaction Chemistry of Pentamethylcyclopentadienyl Cyclooctatetraenyl Uranium Metallocenes. *Chem. Eur. J.* **2011**, *17*, 4871−4878.
(80) Palumbo, C. T.; Fieser, M. E.; Ziller, J. W.; Evans, W. J. Reactivity of Complexes of $4f^n5d^1$ and $4f^{n+1}$ Ln^{2+} Ions with Cyclooctatetraene. *Organometallics* **2017**, *36*, 3721−3728.
(81) Palumbo, C. T.; Darago, L. E.; Dumas, M. T.; Ziller, J. W.; Long, J. R.; Evans, W. J. Structure, Magnetism, and Multi-Electron Reduction Reactivity of the Inverse Sandwich Reduced Arene La^{2+} Complex $[\{[C_5H_3(SiMe_3)_2]_2La\}(\mu\text{-}\eta^6\text{:}\eta^6\text{-}C_6H_6)]^{1-}$. *Organometallics* **2018**, *37*, 3322−3331.
(82) Feltham, H. L. C.; Brooker, S. Review of Purely 4*f* and Mixed-Metal nd-4*f* Single-Molecule Magnets Containing Only One Lanthanide Ion. *Coord. Chem. Rev.* **2014**, *276*, 1−33.
(83) Kahn, O. *Molecular Magnetism*; VCH: 1993.
(84) Rinehart, J. D.; Long, J. R. Exploiting Single-Ion Anisotropy in the Design of f-Element Single-Molecule Magnets. *Chem. Sci.* **2011**, *2*, 2078−2085.
(85) Chilton, N. F.; Collison, D.; McInnes, E. J. L.; Winpenny, R. E. P.; Soncini, A. An Electrostatic Model for the Determination of Magnetic Anisotropy in Dysprosium Complexes. *Nat. Commun.* **2013**, *4*, 2551.
(86) Demir, S.; Zadrozny, J. M.; Long, J. R. Large Spin-Relaxation Barriers for the Low-Symmetry Organolanthanide Complexes $[Cp^*_2Ln(BPh_4)]$ (Cp^*=pentamethylcyclopentadienyl; Ln = Tb, Dy). *Chem. Eur. J.* **2014**, *20*, 9524−9529.
(87) Demir, S.; Boshart, M. D.; Corbey, J. F.; Woen, D. H.; Gonzalez, M. I.; Ziller, J. W.; Meihaus, K. R.; Long, J. R.; Evans, W. J. Slow Magnetic Relaxation in a Dysprosium Ammonia Metallocene Complex. *Inorg. Chem.* **2017**, *56*, 15049−15056.
(88) Errulat, D.; Gabidullin, B.; Mansikkamäki, A.; Murugesu, M. Two Heads Are Better than One: Improving Magnetic Relaxation in the Dysprosium Metallocene upon Dimerization by Use of an Exceptionally Weakly-Coordinating Anion. *Chem. Commun.* **2020**, *56*, 5937−5940.
(89) Meng, Y. S.; Zhang, Y. Q.; Wang, Z. M.; Wang, B. W.; Gao, S. Weak Ligand-Field Effect from Ancillary Ligands on Enhancing Single-Ion Magnet Performance. *Chem. Eur. J.* **2016**, *22*, 12724−12731.
(90) Goodwin, C. A. P.; Reta, D.; Ortu, F.; Chilton, N. F.; Mills, D. P. Synthesis and Electronic Structures of Heavy Lanthanide Metallocenium Cations. *J. Am. Chem. Soc.* **2017**, *139*, 18714−18724.
(91) Krishnan, R.; Binkley, J. S.; Seeger, R.; Pople, J. A. Self-consistent Molecular Orbital Methods. XX. A Basis Set for Correlated Wave Functions. *J. Chem. Phys.* **1980**, *72*, 650−654.
(92) Schleyer, P. v. R.; Maerker, C.; Dransfeld, A.; Jiao, H.; van Eikema Hommes, N. J. R. Nucleus-Independent Chemical Shifts: A Simple and Efficient Aromaticity Probe. *J. Am. Chem. Soc.* **1996**, *118*, 6317−6318.

https://doi.org/10.1021/acs.inorgchem.1c03230
Inorg. Chem. 2022, 61, 2444−2454